Journal of Sound and Vibration (2001) **245**(5), 815–834
doi:10.1006/jsvi.2001.3597, available online at http://www.idealibrary.com on IDEAL®

MODELLING OF DYNAMIC RESPONSES OF AN AUTOMOTIVE FUEL RAIL SYSTEM, PART II: ENTIRE SYSTEM

S. F. Wu and Q. Hu

Department of Mechanical Engineering, Wayne State University, Detroit, MI 48202, *U.S.A.*

and

S. Stottler and R. Raghupathi

Robert Bosch Corporation, 38000 *Hills Tech Drive, Farmington Hills, MI* 48331-3417, *U.S.A.*

(*Received* 1 *June* 1999, *and in final form* 22 *December* 2000)

The computer model developed for calculating pressure fluctuations inside an automotive fuel injector (Hu *et al. Journal of Sound and Vibration* (submitted)) is extended to the entire fuel rail system, which consists of six injectors, a pressure regulator, pressure damper, fuel pump, and torturous fuel supply and return lines. Since the pressure fluctuations generated inside any injector can propagate throughout the entire fuel rail system, the responses of all injectors are coupled. The presence of a pressure regulator may also affect the dynamic responses of the fuel rail system. In Part II of this paper, formulations for describing pressure fluctuations inside the injectors, pressure regulator, and fuel rails are derived and solved simultaneously. The effect of twists and turns of the fuel lines on the losses of fluid kinetic energy, and that of wave propagation throughout the fuel rail system are taken into account. The computer model thus developed is validated experimentally. Measurements are conducted on a test bench that simulates a real engine with injectors fired in a particular order. The calculated pressure fluctuations inside different injectors and fuel lines are compared with the measured data under various working conditions. Favorable agreements are obtained in all cases.

1. INTRODUCTION

In Part I of this paper, the authors [1] developed a computer model for predicting pressure fluctuations inside an automotive fuel injector. There the injector was divided into three segments with a filter at the top, a coil spring and needle assembly in the middle, and orifices at the bottom. The fuel flowing through these segments was assumed to be unsteady, viscous, and one-dimensional. The losses of fluid kinetic energy as the fluid enters the filter at the top and discharges through orifices at the bottom of the injector were described by two loss factors. The former was determined experimentally while the latter was correlated to the motion of the solenoid and needle assembly, which was governed by a second order ordinary differential equation (ODE). Moreover, the pressure fluctuations were required to satisfy a one-dimensional damped wave equation. The dynamic responses of an injector were subsequently determined by solving a set of nine simultaneous equations.

In Part II of this paper, we extend these formulations to the entire automotive fuel rail system, which consists of six injectors, a pressure regulator, fuel pump, and inlet and outlet

0022-460X/01/350815 + 20 $35.00/0

fuel lines with twists and turns. The injectors are fired in a particular order synchronizing with the engine speed. Since the pressure fluctuations induced by opening and closing the solenoid and needle assembly inside any injector may propagate throughout the entire fuel rail, the responses of all injectors are coupled together. The presence of a pressure regulator may also influence the dynamic responses of a fuel rail system. The major component of a pressure regulator is the spring–diaphragm–ball assembly that reacts to the pressures acting on the diaphragm. When the incoming pressure exceeds that of the coil spring, the diaphragm is pushed up to allow for more fluid flow. As the flow velocity increases, the incoming pressure drops and the coil spring pushes the diaphragm back. Consequently, the fluid pressure inside the fuel rail is maintained at a constant level. The twists and turns of the fuel supply and return lines also have a direct impact on the resulting responses of the system. These effects are all considered in Part II of this paper.

2. MODELLING OF FUEL RAILS AND INJECTORS

The flow field inside an automotive fuel rail system is much more complex than that inside an injector. Figure 1 shows a typical fuel rail system, which includes six injectors and a pressure regulator connected by torturous fuel lines. Because the injectors are connected in series, pressure fluctuations generated inside one injector may propagate throughout the entire fuel rail and influence the responses of others. The flow fields are further complicated by sharp twists and turns of the fuel lines, which may have a direct impact on the losses of

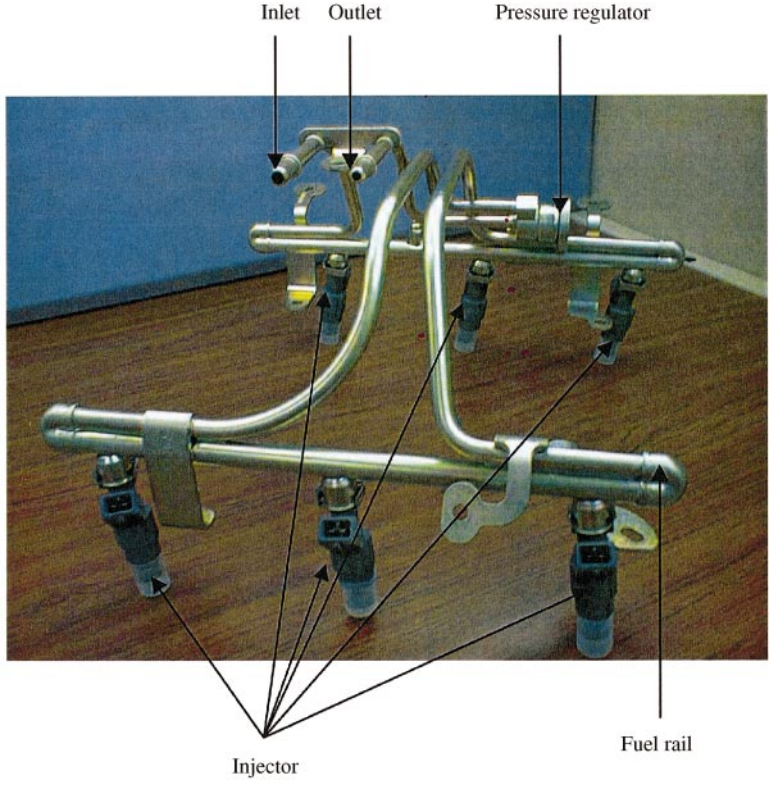

Figure 1. An automotive fuel rail system containing six injectors, pressure regulator, and torturous fuel lines.

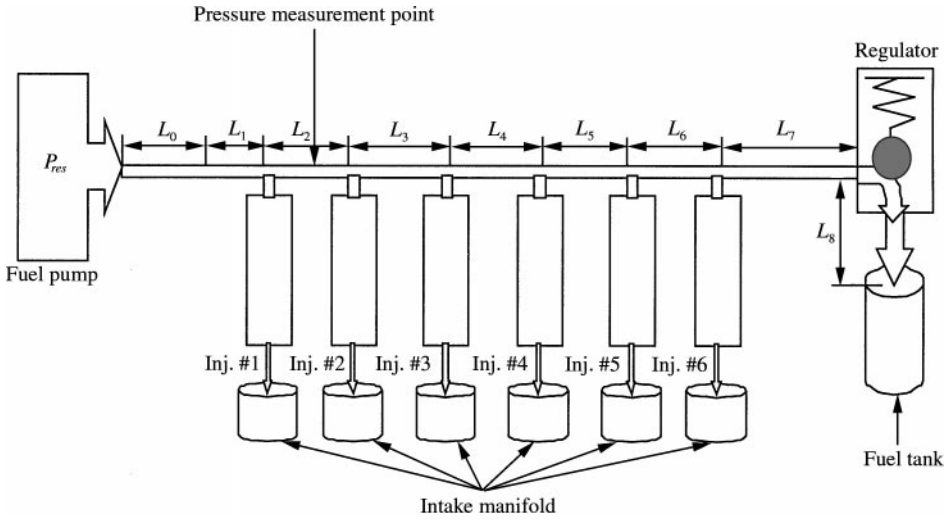

Figure 2. Schematic of the automotive fuel rail system under consideration.

fluid kinetic energy. To account for these coupling and wave propagation effects, it is necessary to consider the whole fuel rail system and solve the dynamic responses of all injectors and pressure regulator simultaneously.

Figure 2 illustrates a schematic of the fuel rail system under consideration. The injectors are numbered 1–6 in sequence so as to facilitate a shorthand notation of mathematical formulations. This numbering system may be different from the conventional one, favored by the practicing engineers, which usually indicates a specific engine firing order. Under the present numbering system, the fuel discharged from the pump flows through injectors 1–6 in sequence and then passes the pressure regulator to the fuel return line.

To facilitate numerical computations, the fuel lines are discretized into segments defined as follows. The segment connecting the fuel pump and inlet is termed as line 0, that connecting the inlet to the first injector as line 1, those between injectors $(i-1)$ and i as line i, $i = 2$–6, that between the sixth injector and pressure regulator as line 7, and that connecting the pressure regulator to the fuel return as line 8. To account for the losses of fluid kinetic energy through each of the line segments, loss factors are introduced and indexed in the same manner as those of the line segments. Note that all line segments are assumed straight as shown in Figure 2. The losses of fluid kinetic energy due to twists and turns of the fuel line are accounted for by the loss factors based on the notion of an equivalent length of a straight-line segment [2].

The injectors connected in series are modelled in a similar manner as those of a single injector [1]. Assume that the fluid is homogeneous and incompressible and that fuel flowing through each line segment is unsteady and one-dimensional. Then we can describe the pressures and velocities in all components of the fuel rail system as [3, 4]

$$P_{pump} = P_{0,end} + \tfrac{1}{2}\rho V_{0,end}^2 + \tfrac{1}{2}\rho K_0 V_{0,end}^2, \tag{1a}$$

$$P_{n,end} + \tfrac{1}{2}\rho V_{n,end}^2 = P_{(n+1),end} + \tfrac{1}{2}\rho V_{(n+1),end}^2 + \tfrac{1}{2}\rho K_{(n+1)} V_{(n+1),end}^2 \quad (n = 1, \ldots, 6), \tag{1b}$$

$$P_{reg,ent} + \tfrac{1}{2}\rho V_{7,end}^2 = P_{reg,ext} + \tfrac{1}{2}\rho V_{8,end}^2 + \tfrac{1}{2}\rho(K_{reg,ent}V_{reg,ent}^2 + K_{reg,tur}V_{reg,tur}^2 + K_{reg,ext}V_{reg,ext}^2), \tag{1c}$$

$$P_{reg,ext} + \tfrac{1}{2}\rho V_{8,end}^2 = P_{out} + \tfrac{1}{2}\rho K_8 V_{out}^2, \tag{1d}$$

where P_{pump} represents the input pressure from the fuel pump; P_{out} and V_{out} are the pressure and flow velocity at the fuel return lines; $P_{n,end}$ and $V_{n,end}$ indicate the pressure and flow velocity at the end of the nth line segment ($n = 0, 1, \ldots, 8$); K_n is the corresponding loss factor for the fluid flowing through the nth line segment; $P_{reg,ent}$, $P_{reg,tur}$, $P_{reg,ext}$, $V_{reg,ent}$, $V_{reg,tur}$, $V_{reg,ext}$, $K_{reg,ent}$, $K_{reg,tur}$, and $K_{reg,ext}$ stand for the pressures, flow velocities, and loss factors at the entrance, turning section, and exit of the regulator, respectively; and ρ is the fluid density.

Attached to the ends of line segments 1–6 are six injectors. The flow fields inside these injectors can be described by the following equations [1]:

$$P_{n,end} + \tfrac{1}{2}\rho V_{n,end}^2 = P_{n,T} + \tfrac{1}{2}\rho(V_{n,T}^2 + K_{n,F}V_{n,F}^2), \tag{2a}$$

$$P_{n,T} + \frac{1}{2}\rho V_{n,T}^2 = P_{n,B} + \frac{1}{2}\rho V_{n,B}^2 + \rho h\frac{\mathrm{d}V_{n,av}}{\mathrm{d}t}, \tag{2b}$$

$$P_{n,B} + \frac{1}{2}\rho V_{n,B}^2 + \rho h\frac{\mathrm{d}V_{n,av}}{\mathrm{d}t} = P_{out} + \frac{1}{2}\rho K_{n,O}V_{n,O}^2, \tag{2c}$$

where $n = 1$–6, $P_{n,T}$ and $P_{n,B}$ represent the pressures at the top and the bottom sections of the nth injector, respectively; $V_{n,T}$ and $V_{n,B}$ are the flow velocities at the corresponding locations; $K_{n,F}$ and $K_{n,O}$ are the loss factors for the dynamic pressure head as fluid enters the injector through the filter at the top and discharges into the cylinder chamber through four orifices at the bottom of the injector, respectively; $V_{n,F}$ and $V_{n,O}$ are the flow velocities at the corresponding locations; $V_{v,an}$ is the average flow velocity inside the nth injector; and h is the length of the injector.

Since the filters inside injectors are fixed, the loss factors $K_{n,F}$ can be assumed constant. Their values can be determined by measuring the pressures and volume flows through the filters, given the cross-sectional areas of the injectors [1]. The loss factors $K_{n,O}$ are correlated to the needle displacements x_n measured with respect to the valve seats of the injectors. Based on the theory of internal flows through a sudden expansion chamber [4], we can write $K_{n,O}$ as

$$K_{n,O} = 1 + \left(\frac{A_{n,O}}{x_n D_n}\right)^2 \begin{cases} \left(1 - \dfrac{x_n D_n}{A_{n,B}}\right)^2, & x_n \leqslant \dfrac{A_{n,B}}{D_n}, \\ \left(1 - \dfrac{A_{n,B}}{x_n D_n}\right)^2, & x_n > \dfrac{A_{n,B}}{D_n}, \end{cases} \tag{3}$$

where D_n is the diameter of the bottom section inside the nth injector and x_n satisfies the equation of motion

$$m_n\ddot{x}_n + c_0\dot{x}_n + k_n x_n = -f_{n,p} + f_{n,m}, \tag{4}$$

where m_n and k_n represent the lumped mass and spring constant of the needle for the nth injector, respectively; and $f_{n,p}$ and $f_{n,m}$ are the corresponding spring pre-loading and magnetic forces acting on the needle respectively. The value of $f_{n,p}$ is usually specified and that of $f_{n,m}$ can be approximated by an empirical formula [1].

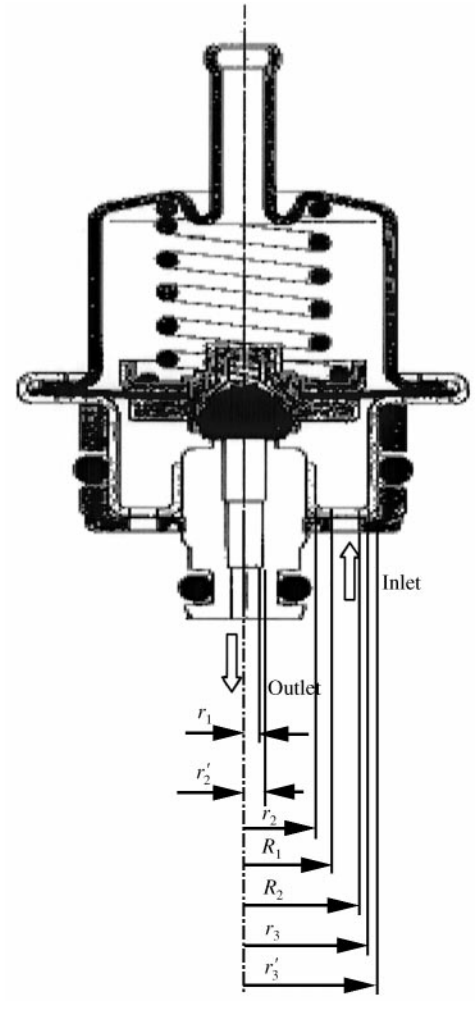

Figure 3. Cross-sectional view of a pressure regulator.

3. MODELLING OF PRESSURE REGULATOR

The major component of a pressure regulator is the spring–diaphragm–ball assembly that reacts to the pressures acting on both sides of the diaphragm. Figure 3 shows a cross-section of an assembled pressure regulator. Figure 4 depicts a schematic of a regulator to illustrate the force balance of the spring–diaphragm–ball assembly. Here the ball at the center is represented by a sphere of mass m_{ball}. The effective displacement of the ball is indicated by x_{ball}. The effective spring constant acting on the ball is $k_{eff} = k_c + k_m$, which is the sum of contributions from a coil spring k_c and diaphragm k_m. The pressures and velocities at the entrance and exit of the regulator are denoted by $P_{reg,ent}$, $V_{reg,ent}$, $P_{reg,ext}$, and $V_{reg,ext}$ respectively (see Figure 4). When the pressure of the inlet flow $P_{reg,ent}$ is larger than that of the spring, the diaphragm is pushed upwards, allowing more fluid to pass through with pressure $P_{reg,ext}$ and velocity $V_{reg,ext}$. As the flow velocity increases, the inlet pressure $P_{reg,ent}$ decreases so the coil spring pushes the diaphragm back until the forces on both sides of the diaphragm are balanced.

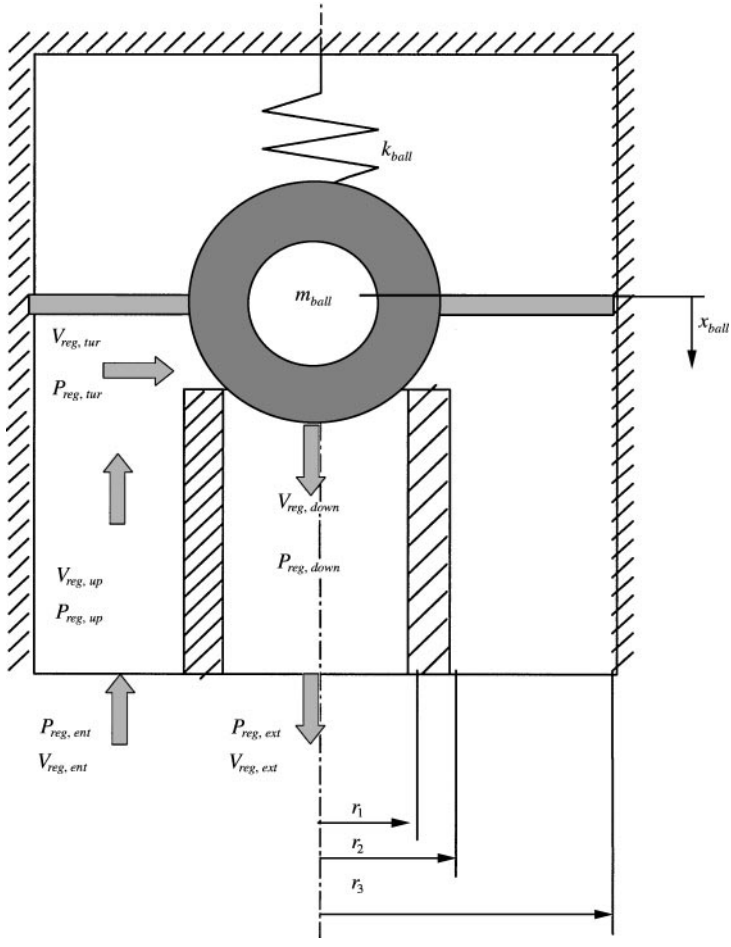

Figure 4. Schematic of the pressure regulator under consideration.

In modelling the responses of a pressure regulator, we divide the flow field into three regions: upstream, downstream, and turning point around the spring–diaphragm–ball assembly. According to Bernoulli's equation [3] with consideration of the loss of kinetic energy [4], the equations governing pressures and velocities in these regions can be written as

$$P_{reg,ent} + \tfrac{1}{2}\,\rho V_{reg,ent}^2 = P_{reg,up} + \tfrac{1}{2}\,\rho V_{reg,up}^2 + \tfrac{1}{2}\,\rho K_{reg,ent}\,V_{reg,ent}^2, \tag{5a}$$

$$P_{reg,up} + \tfrac{1}{2}\,\rho V_{reg,up}^2 = P_{reg,tur} + \tfrac{1}{2}\,\rho V_{reg,tur}^2, \tag{5b}$$

$$P_{reg,tur} + \tfrac{1}{2}\,\rho V_{reg,tur}^2 = P_{reg,down} + \tfrac{1}{2}\,\rho V_{reg,down}^2 + \tfrac{1}{2}\,\rho K_{reg,tur}\,V_{reg,tur}^2, \tag{5c}$$

$$P_{reg,down} + \tfrac{1}{2}\,\rho V_{reg,down}^2 = P_{reg,ext} + \tfrac{1}{2}\,\rho V_{reg,out}^2 + \tfrac{1}{2}\,\rho K_{reg,ext}\,V_{reg,ext}^2, \tag{5d}$$

where $P_{reg,up}$, $V_{reg,up}$, $P_{reg,down}$, and $V_{reg,down}$ are the pressures and flow velocities in the upstream and downstream regions, respectively; $P_{reg,tur}$, and $V_{reg,tur}$ are the pressure and flow velocity at the turning point around the spring–diaphragm–ball assembly, respectively; and $K_{reg,ent}$ and $K_{reg,tur}$ account for the losses of fluid kinetic energy as the fluid enters the

regulator and passes the turning point, respectively, which are given by

$$K_{reg,ent} = \left[1 - \left(\frac{A_{ent}}{A_{up}}\right)\right]^2, \quad (A_{ent} < A_{up}), \tag{6a}$$

$$K_{reg,tur} = \left[1 - \left(\frac{A_{tur}}{A_{down}}\right)\right]^2, \quad (A_{tur} < A_{down}), \tag{6b}$$

where the cross-sectional areas A_{ent}, A_{up}, A_{tur}, and A_{down} at the entrance, upstream, turning point, and downstream of a pressure regulator, respectively:

$$A_{ent} = \gamma\pi(R_2^2 - R_1^2), \qquad A_{up} = \gamma\pi(r_3^2 - r_2^2), \qquad A_{tur} = \pi(r_1 + r_2')x_{ball}, \qquad A_{down} = \pi r_1^2, \tag{7a–d}$$

where $\gamma = A_{free}/A_{ring}$ is the ratio of the cross-sectional area of flow passage to that of the ring bounded by R_2 and R_1. The value of γ is constant for a given pressure regulator. The radii R_i, r_i and r_i' in equation (7) are indicated in Figures 3 and 4 respectively.

Note that $K_{reg,ext}$ in equation (5d) indicates the loss of the kinetic energy as fluid exits the regulator. For simplicity, we set $K_{reg,ext} = 1$ and $V_{reg,ext} = V_{reg,down}$ because the cross-sectional areas of the fuel lines are equal at the joint between the regulator exit and fuel return. The variable x_{ball} in equation (7c) is the effective displacement of the ball that controls the flow rate inside the fuel rail system. Because of a dependence on x_{ball} [see equations (6b) and (7c)], the loss factor $K_{reg,tur}$ is a function of the motion of the spring–diaphragm–ball assembly, which is governed by the following second order ODE:

$$m_{ball}\ddot{x}_{ball} + c_{eff}\dot{x}_{ball} + k_{eff}x_{ball} = -f_{pr} + P_{reg,up}A_{up}' + P_{reg,tur}A_{tur}' + P_{reg,down}A_{down}, \tag{8}$$

where c_{eff} and k_{eff} are the effective viscous damping coefficient and stiffness of the assembly, f_{pr} is the spring pre-loading force acting on the ball, and A_{up}' and A_{tur}' are given by

$$A_{up}' = \pi(r_3'^2 - r_2'^2), \qquad A_{tur}' = \pi(r_2'^2 - r_1^2). \tag{9a, b}$$

Since the diaphragm and the coil spring undergo the same amount of displacement when the spring–diaphragm–ball assembly is pushed upwards, the effective spring constant k_{eff} in equation (8) can be written as

$$k_{eff} = k_c + k_m. \tag{10}$$

The value of k_c can be determined experimentally by measuring the linear deformations Δ of the spring under different weights W. The slope of this line is the spring constant, $k_c = W/\Delta$. The stiffness of the diaphragm k_m is much more difficult to determine than that of the coil spring k_c. This is because the diaphragm is made of composite materials. The rate of change in Young's modulus (slope) of the reinforcing fabric material is not only non-linear, but also different in both warp and woof directions with respect to the deformations of the material. Test results show that when the deformations are small, for example within 2 per cent in either warp or woof direction, the rate of change in Young's modulus is constant. When the deformations exceed 2 per cent, the slopes of Young's moduli decrease with the increase of the deformations of the reinforcing fabric materials in both directions. At around 10 per cent of the deformations, the slopes of Young's moduli start to increase, and gradually approach constant values again at very large deformations.

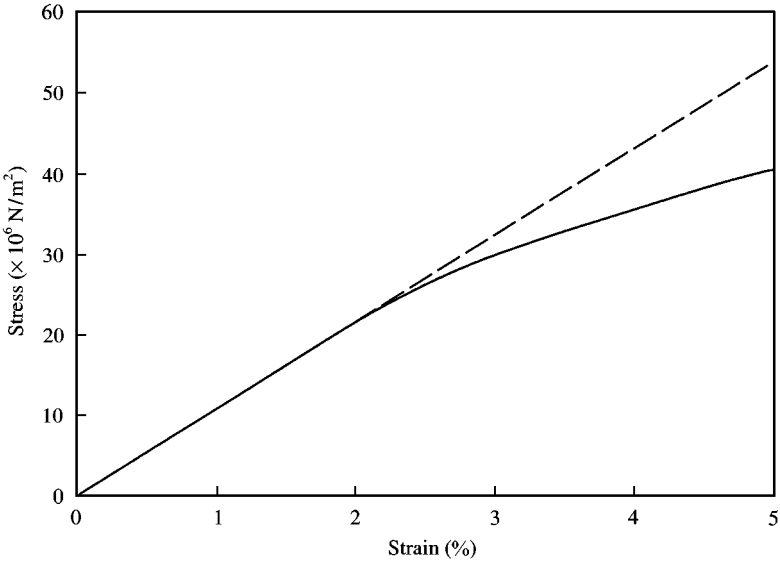

Figure 5. Linearization of the resultant stiffness of the diaphragm inside the pressure regulator: ——, measured; – – –, simulated.

In this investigation, we assume that the deformation of the diaphragm remains small (less than 2 per cent) at all times, so that the resultant stress–strain relation of the diaphragm can be linearized (see Figure 5). Under this condition, we can use an empirical formula to estimate the spring constant for a diaphragm with clamped–lumped mass boundary conditions [5]:

$$k_m = \frac{\delta^3 E}{\kappa a^2}, \tag{11}$$

where E and δ are the resultant Young's modulus and thickness of the diaphragm, respectively; κ is a constant depending upon the ratio of the radius of the diaphragm a and the width of the lumped mass b. For the pressure regulator under consideration, the ratio $a/b = 1{\cdot}326$. Therefore $\kappa = 0{\cdot}00284$ [5].

The exact value of the effective viscous damping coefficient c_{eff} for the spring–diaphragm–ball assembly is unknown. However, numerical results indicate that the response of the pressure regulator is relatively insensitive to c_{eff}. Hence we set $c_{eff} = 10$ (N s/m) for the sake of convenience. In numerical computations, the dimensions of a pressure regulator must be specified. Table 1 lists typical dimensions and relevant constants for the pressure regulator under consideration as the input to the computer model.

4. CONSERVATION OF MASS

The fluid flowing through a fuel rail system must satisfy the conservation of mass law [6]. Applying this law to each individual line segment, injector, and pressure regulator (see Figures 2 and 4), we obtain

$$V_{0,end} S_0 = V_{1,beg} S_1, \tag{12a}$$

TABLE 1

Input data for the pressure regulator under consideration

Parameters	Descriptions
R_1	Radius (see Figure 3)
R_2	Radius (see Figure 3)
r_1	Radius (see Figure 3)
r_2	Radius (see Figure 3)
r_3	Radius (see Figure 3)
r_2'	Radius (see Figure 3)
r_3'	Radius (see Figure 3)
γ	Flow passage cross-sectional area ratio
m_{ball}	Mass of the ball
f_{pr}	Pre-loading spring force acting on the ball
a	Radius of the diaphragm
b	Width of the lumped mass
δ	Thickness of the diaphragm
k_c	Spring constant acting on the ball

TABLE 2

Input of the fuel line segments and the corresponding cross-sectional areas

Parameters	Descriptions
l_0	Length of fuel line segment connecting pump and inlet
l_1	Length of fuel line segment between inlet and first injector
l_2	Length of fuel line segment between first and second injector
l_3	Length of fuel line segment between second and third injector
l_4	Length of fuel line segment between third and fourth injector
l_5	Length of fuel line segment between fourth and fifth injector
l_6	Length of fuel line segment between fifth and sixth injector
l_7	Length of fuel line segment between sixth and regulator
l_8	Length of fuel line segment between regulator and outlet
S_0	Cross-sectional area of the fuel line segment l_0
S_1	Cross-sectional area of the fuel line segment l_1
S_2	Cross-sectional area of the fuel line segment l_2
S_3	Cross-sectional area of the fuel line segment l_3
S_4	Cross-sectional area of the fuel line segment l_4
S_5	Cross-sectional area of the fuel line segment l_5
S_6	Cross-sectional area of the fuel line segment l_6
S_7	Cross-sectional area of the fuel line segment l_7
S_8	Cross-sectional area of the fuel line segment l_8

$$V_{n,end}S_n = V_{(n+1),beg}S_{(n+1)} + V_{n,T}A_{n,T} \quad (n = 1, 2, \ldots, 6), \tag{12b}$$

$$V_{6,end}S_6 = V_{7,beg}S_7, \tag{12c}$$

$$V_{7,end}S_7 = V_{reg,ent}A_{ent} = V_{reg,up}A_{up} = V_{reg,tur}A_{tur} = V_{reg,down}A_{down} = V_{reg,ext}A_{ext} \tag{12d}$$

$$V_{n,F}A_{n,F} = V_{n,T}A_{n,T}, \quad V_{n,B}A_{n,B} = V_{n,O}A_{n,O} \quad (n = 1, 2, \ldots, 6), \tag{12e}$$

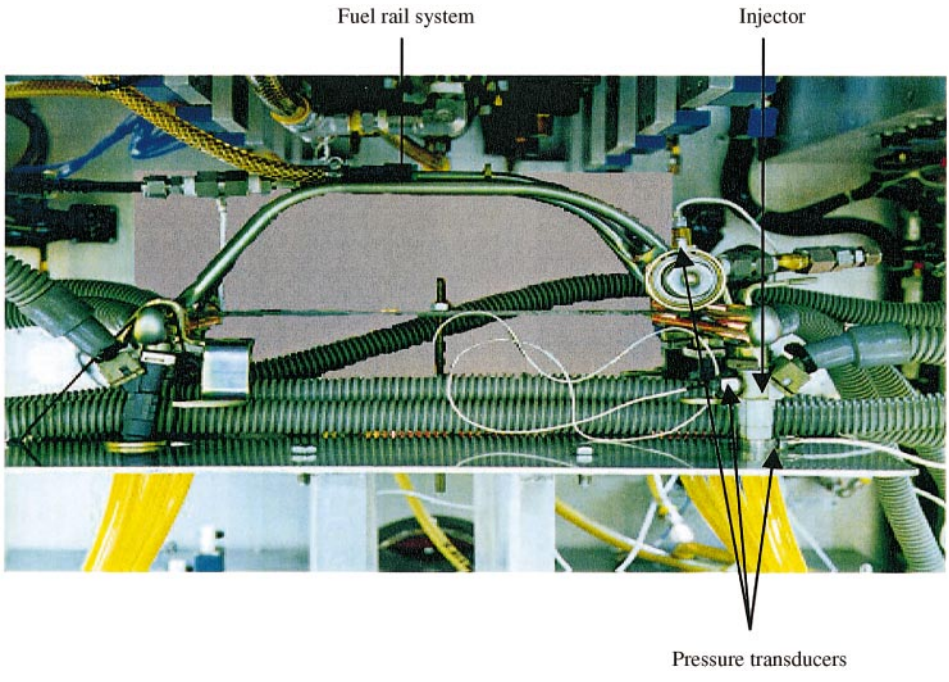

Figure 6. Measurement set-up of the fuel rail system on a test bench simulating a full-size vehicle.

where S_n, $n = 0, 1, \ldots, 8$ are the cross-sectional areas of the nth segment of the line segment; $V_{n,beg}$ are the corresponding flow velocities at the beginning of the nth line segment; $A_{n,F}$, $A_{n,T}$, $A_{n,B}$, and $A_{n,O}$ are the cross-sectional areas at the entrance, top and bottom sections, and orifices of the nth injector, respectively; A_{ent}, A_{up}, A_{tur}, A_{down}, and A_{ext} are the cross-sectional areas at the entrance, upstream, turning point, downstream, and exit of the pressure regulator respectively. The average flow velocity inside the nth injector is given by

$$V_{n,av} A_{n,av} = V_{n,O} A_{n,O} \quad (n = 1, 2, \ldots, 6), \tag{13}$$

where $A_{n,av}$ is the average cross-sectional area of the nth injector.

Note that in this case the injectors are identical. Therefore, they have the same needle mass m and spring constant k, and subject to the same magnitudes of excitation forces f_p and f_{mn}. However, they are located at different locations along the fuel rail system under a particular firing order. Consequently, the coupling effect on each individual injector may be different. For example, the coupling of all injectors on the first injector may be different from that on the second one.

5. EFFECT OF WAVE PROPAGATION

The pressure fluctuations generated inside any injector can propagate throughout the entire fuel rail and affect the responses of other injectors. The propagation of these pressure fluctuations can be described by a damped wave equation, obtained by applying the Navier–Stokes equation [7] to the one-dimensional laminar flow of a Newtonian fluid, using the conservation of mass or continuity equation [8] and the thermodynamic

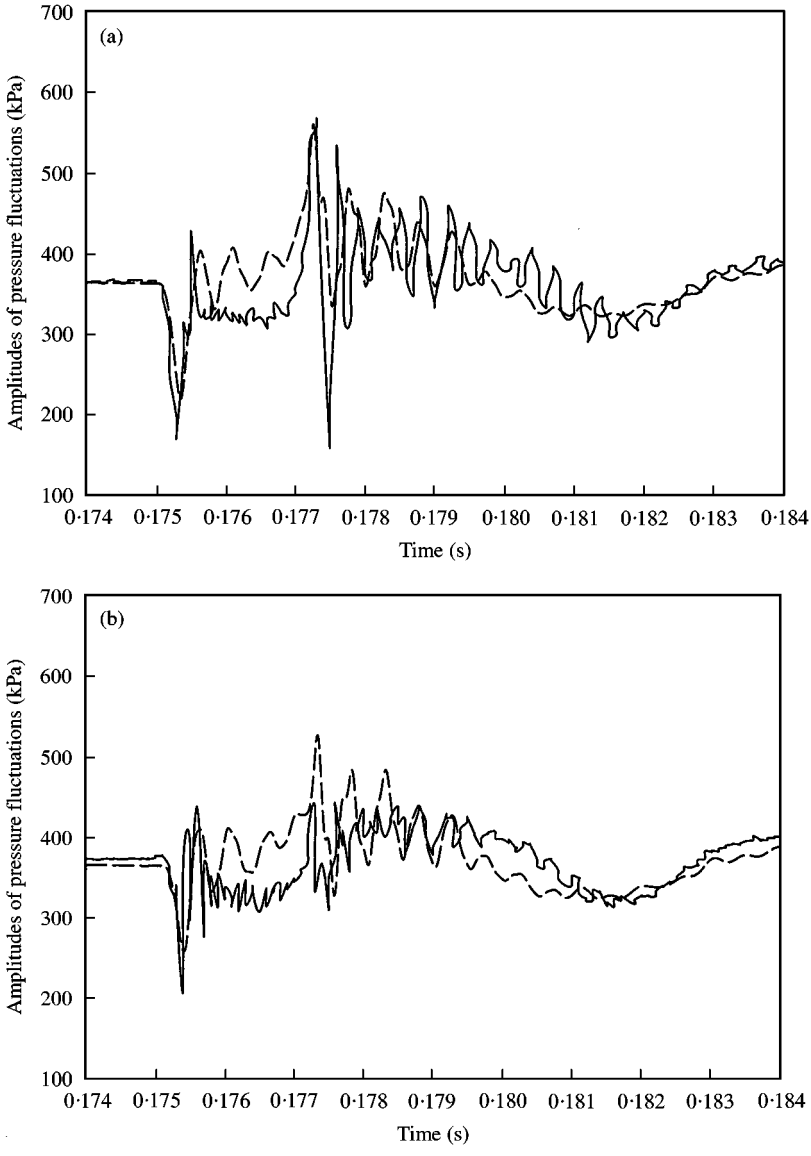

Figure 7. Comparison of pressure fluctuations inside the second injector with the second injector open only: (a) bottom; (b) top; ——, measured; – – –, calculated.

equation [9], and neglecting the high order term

$$\frac{\partial^2 P}{\partial y^2} - \frac{1}{c^2}\frac{\partial^2 P}{\partial t^2} = -\frac{v}{c^2}\frac{\partial^3 P}{\partial t \partial y^2}, \tag{14}$$

where P represents pressure fluctuations; t the time; y the co-ordinate in the flow direction; c the sound speed in the fluid; and v the kinematic viscosity. Equation (14) governs the pressure fluctuations inside all injectors, pressure regulator, and line segments of the fuel rail system under consideration. These pressure fluctuations are correlated to flow velocities by

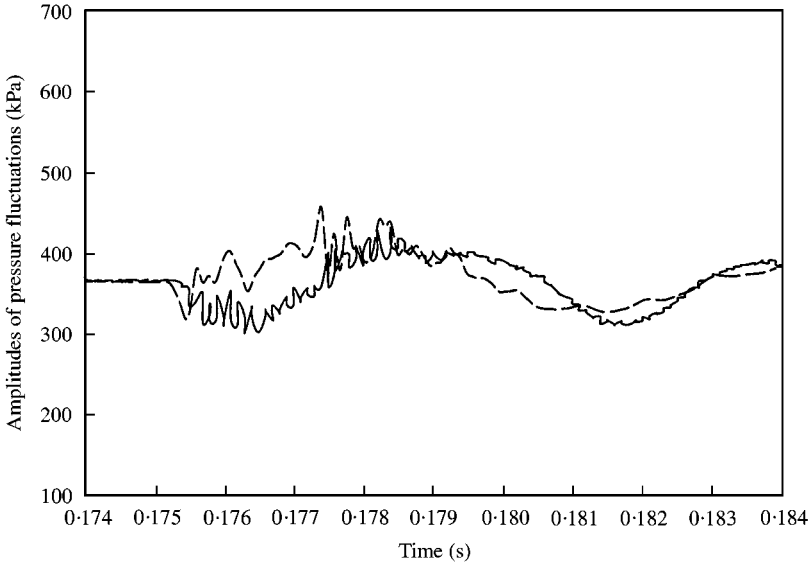

Figure 8. Comparison of pressure fluctuations inside the fuel line segment 2 with the second injector open only: ——, measured; – – –, calculated.

a linearized momentum equation [1]

$$\frac{\partial V}{\partial y} = -\frac{1}{\rho c^2}\frac{\partial P}{\partial t}. \tag{15}$$

Equations (1)–(15) completely define the responses of the fuel injection system under consideration. These equations are solved simultaneously. In particular, the wave equation (14) is solved by using a finite (backward) difference method [8], with pressure boundary conditions specified at the fuel pump P_{pump}, and all the return fuel line segments P_{out} (see Figure 2). An iterative scheme is used to limit the numerical computation errors to a pre-determined level at each time step. Table 2 lists the input variables for the fuel rail system under consideration.

6. TEST SET-UP

Figure 6 shows the measurement set-up on a test bench simulating the fuel rail system of a full-size vehicle. This set-up consisted of six injectors connected in series, pressure regulator, injector power supply and controller, fuel pump, supply, and return lines. The controller was used to control the firing order and pulse width, namely, the opening and closing times inside each injector. In this investigation, the fuel injection system was fired in the order of 3-6-1-5-2-4 in accordance with the numbering system adopted in this paper, which may be different from the actual firing order because a different numbering system may be used. The pulse width for each injector was kept the same at 2·5 ms. The test fluid was *n*-Heptane, which has the same density and viscosity as those of gasoline, but provides greater stability.

To monitor the pressure fluctuations at various locations of the fuel injection system, several Kulite XT-123C-100 pressure transducers were mounted on the top and bottom

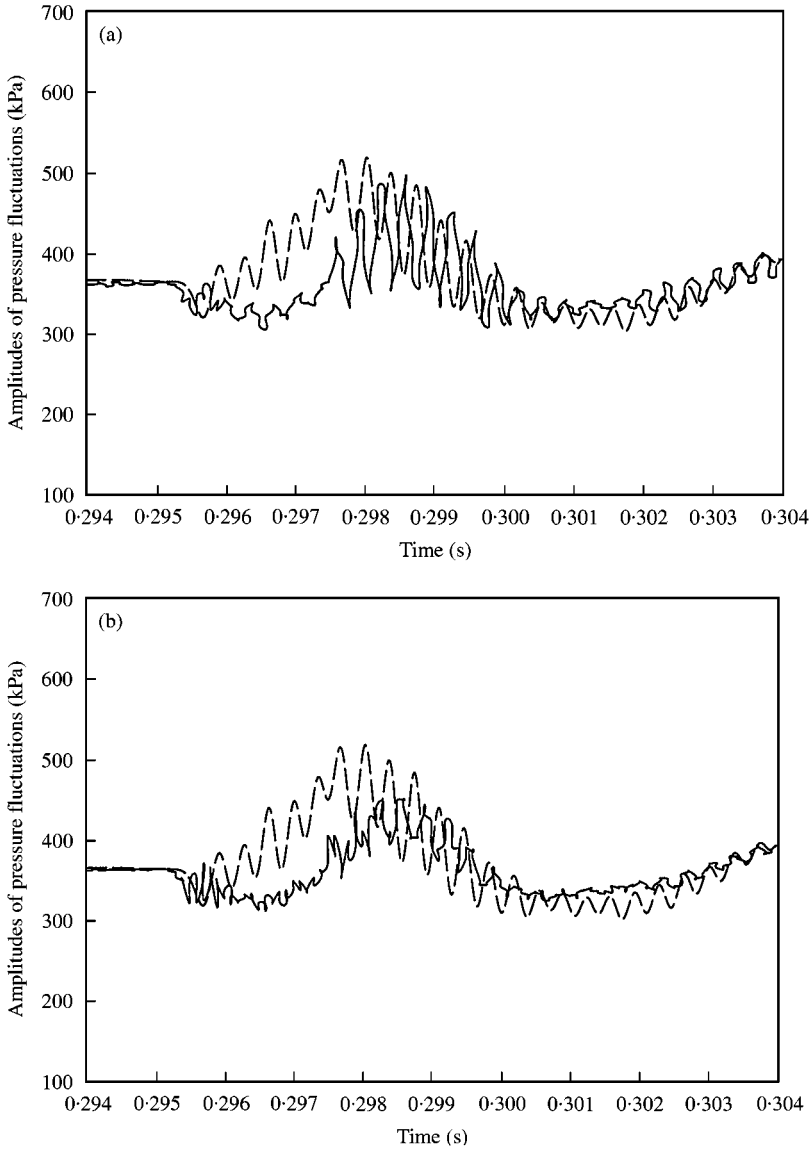

Figure 9. Comparison of pressure fluctuations inside the third injector with the fourth injector open only: (a) bottom; (b) top; ——, measured; – – –, calculated.

sections of various injectors and on the fuel line (see Figure 2). The sampling rate of the measurements was set at 24 kHz. The measured pressure fluctuations were digitized and recorded automatically in a desktop computer for post-processing.

7. RESULTS AND DISCUSSIONS

In this section, we demonstrate comparisons of the calculated and measured pressure fluctuations inside the injections and fuel line. In carrying out numerical computations of wave propagation inside the fuel rail system, each line segment was uniformly discretized

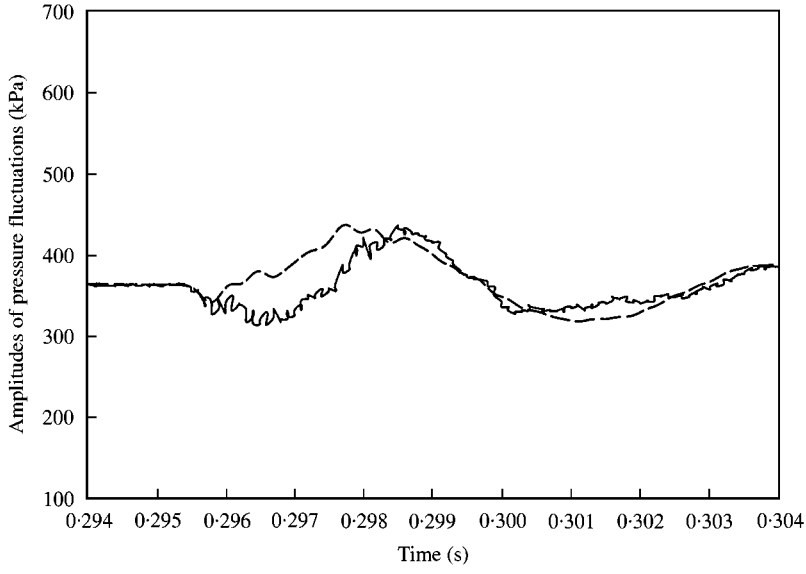

Figure 10. Comparison of pressure fluctuations inside the fuel line segment 2 with the fourth injector open only: ——, measured; – – –, calculated.

into five nodes and each injector into nine nodes. Pressure fluctuations at these nodes were calculated using a finite difference method together with an iteration scheme. The values of pressure fluctuations at these nodes that correspond to the pressure transducers' locations were compared with the measured data.

In this study, five sets of measurements were taken. In the first set, the pressure transducers were installed at the top and bottom sections of the second injector with the second injector being fired. Next, the pressure transducers were moved to the top and bottom sections of the third injector with the fourth injector being fired. This sequence of measurements was then reversed, with the transducers moved to the top and bottom sections of the fourth injector with the third injector being fired. In the last two sets of measurements, pressure fluctuations were measured at the top and bottom sections of the third and second injectors with the sixth and fifth injectors being fired separately respectively. In all these measurements, pressure fluctuations were measured inside the fuel line segment 2 while different injectors were fired separately.

Figure 7 illustrates comparisons of the calculated and measured pressure fluctuations at the bottom and top sections of the second injector with the second injector being fired respectively. Results depict that when the injector is suddenly opened, the pressure experiences an instant drop due to the rarefaction effect. This rarefaction is followed by rapid oscillations whose amplitudes decay exponentially to the ambient level as the injector remains open. When the injector is closed, a pressure surge is generated due to compression, which is known as the "water hammer" phenomenon. The amplitude of the pressure surge decays gradually in an oscillatory manner to the ambient level while the injector remains closed. Results show that the amplitude of pressure surge or drop can be twice as high (or low) as that of the ambient pressure. Hence they are the major causes of metering errors and fuel injection system vibration and noise problems.

Unlike the case of a single injector, the pressures continue to oscillate around its ambient level at a very low frequency after the injector is closed. This phenomenon is caused by the reflections of pressure waves propagating back and forth inside the fuel rail.

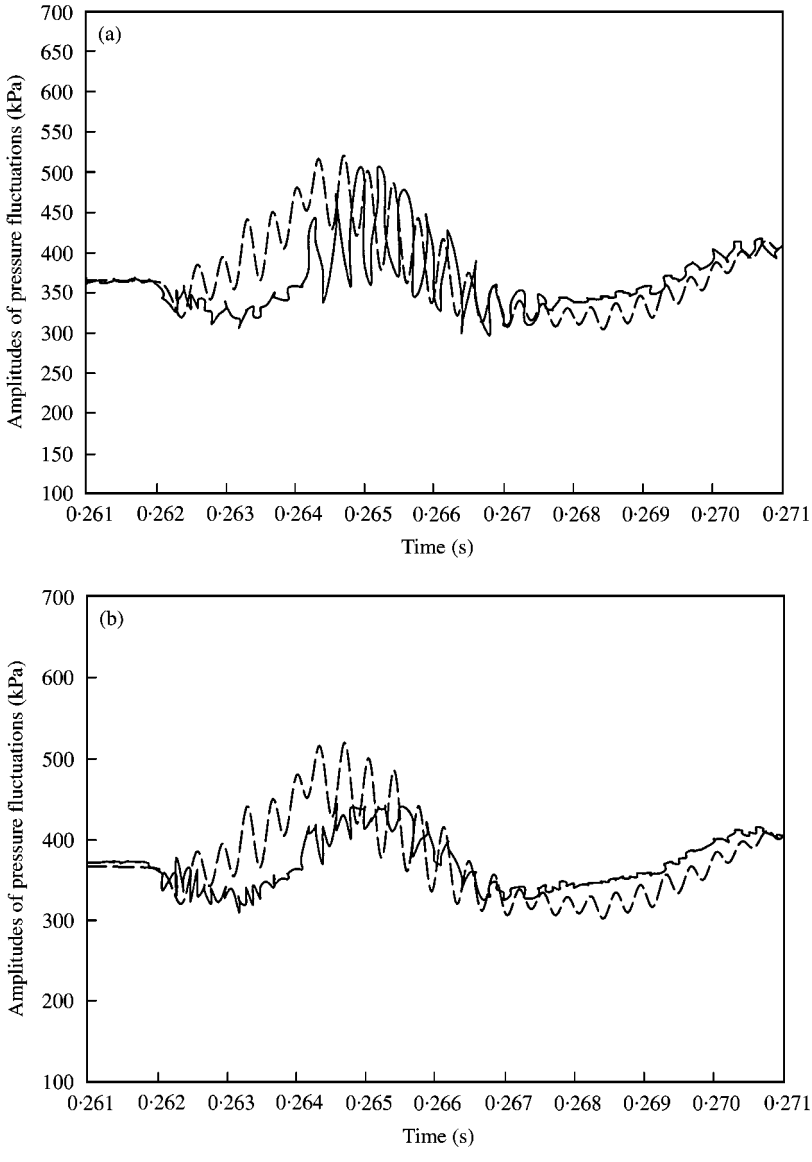

Figure 11. Comparison of pressure fluctuations inside the fourth injector with the third injector open only: (a) bottom; (b) top; ——, measured; – – –, calculated.

Figure 7 shows that the present computer model is capable of capturing the main characteristics of a fuel injection system. In particular, the agreement between the calculated and measured pressure surge at the bottom section when the injector is just closed in almost perfect. However, the calculated amplitude of the pressure drop when the injector is opened is overestimated by 10 per cent. Also, the amplitudes of pressure fluctuations following the pressure drop are overestimated as compared to the measured values. Nonetheless, the trend of pressure fluctuations after the injector is closed agrees well with the measured data. The amplitudes of the calculated pressure fluctuations at the top section of the second injector are overestimated by 10 per cent as compared with the measured data. The reasons

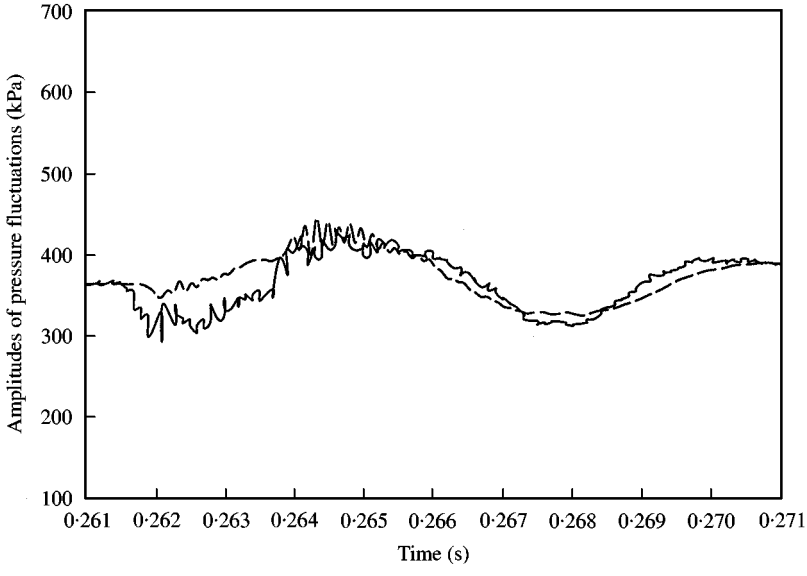

Figure 12. Comparison of pressure fluctuations inside the fuel line segment 2 with the third injector open only: ——, measured; – – –, calculated.

for these discrepancies could be: (1) the locations of the calculated pressure fluctuations may not coincide exactly with those of measurements; (2) the performance of pressure transducers deteriorates at high frequencies, which is why the measured pressures show less oscillations than the calculated values; and (3) the sampling rate of measurements may not be set high enough. As a result, the measured data between 0·1755 and 0·1770 ms seem more like noise than true pressure oscillations.

Figure 8 illustrates the comparison of the calculated and measured pressure fluctuations inside the fuel line segment 2 as the second injector is fired. Here again, discrepancies between the calculated and measured pressure fluctuations are observed after the injector is opened. The general trend of pressure fluctuations after the injector is closed, however, is captured.

Next, we show comparisons of the calculated and measured pressure fluctuations at the bottom and top sections of the third injector with the fourth injector being fired (see Figure 9). The responses in this case are quite different from those of Figure 7. Here we see only smooth oscillations consisting of high- and low-frequency components. These pressure fluctuations can be attributed to the coupling effect. The high-frequency components are caused by the rapid oscillations after the opening and closing of a neighboring injector, while the low-frequency components are due to reflections of the rarefaction and compression waves generated by sudden opening and closing of a neighboring injector from the fuel rail system. The corresponding comparison of pressure fluctuations inside the fuel line segment 2 is shown in Figure 10.

The comparisons of pressure fluctuations at the bottom and top sections of the fourth injector as well as inside the fuel line segment 2 with the third injector being fired are displayed in Figures 11 and 12. The characteristics of these pressure fluctuations are quite similar to those of Figures 9 and 10 as expected. This reciprocity phenomenon holds when the mean flow speed is zero or very low, which is the case when the injectors are closed.

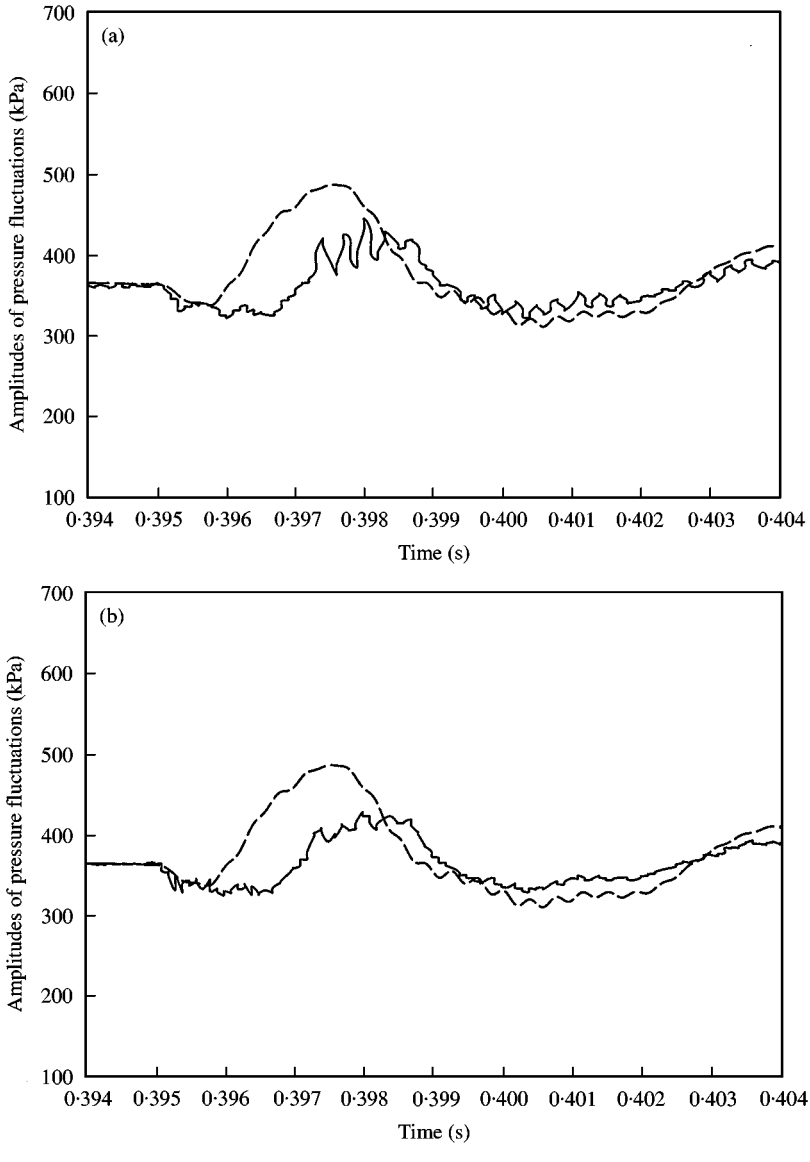

Figure 13. Comparison of pressure fluctuations inside the third injector with the sixth injector open only: (a) bottom; (b) top; ——, measured; – – –, calculated.

Finally, we illustrate comparisons of the calculated and measured pressure fluctuations at the bottom and top sections of the third injector with the sixth injector being fired, and those at the bottom and top sections of the second injector with the fifth injector being fired respectively (see Figures 13 and 15). The corresponding comparisons of pressure fluctuations inside the fuel line segment 2 with the sixth and fifth injectors being fired separately are shown in Figures 14 and 16 respectively.

Note that once the pressure fluctuations are obtained, the flow rate and metering errors through each injector can be calculated. However, because of the difficulties involved in accurately measuring the flow metering errors, such comparisons cannot be made.

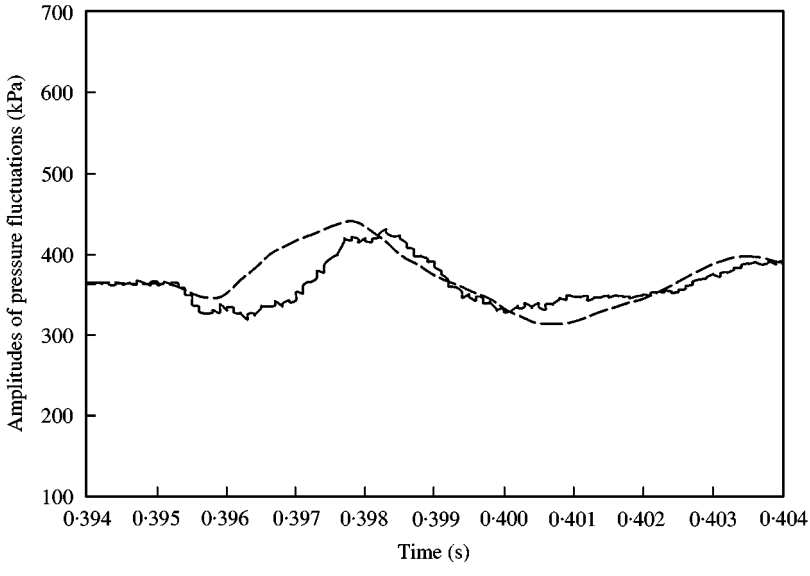

Figure 14. Comparison of pressure fluctuations inside the fuel line segment 2 with the sixth injector open only: ——, measured; – – –, calculated.

8. CONCLUDING REMARKS

A computer model is developed for predicting the dynamic responses of an automotive fuel rail system. In this model, the effects of coupling among the injectors and pressure regulator and those of wave propagation inside the fuel rail system are taken into account. Also, the losses of fluid kinetic energy due to sharp twists and turns of the fuel rail, and those due to the solenoid–needle assembly inside an injector and the spring–diaphragm–ball assembly inside a pressure regulator are considered. The calculated pressure fluctuations inside various injectors and fuel lines are validated experimentally on a test bench that simulates the working conditions of a full–size vehicle. Satisfactory agreements between the calculated and measured pressure fluctuations as the injectors are opened and closed periodically are obtained. Discrepancies between the calculated and measured pressure fluctuations are observed when the injectors remain open. The measured quantities during these times seem more like noise than true pressure fluctuations. This could be due to the deterioration of the pressure transducers' performance in the high-frequency regime or to the fact that the sampling rate of measurements is not high enough.

ACKNOWLEDGMENTS

The authors wish to thank Mr Rick Wolski, Mr Kevin Grabowski, and Mr Ralf Vollmer for assisting with the collection of experimental data in this project. This work was sponsored by the Robert Bosch Corporation.

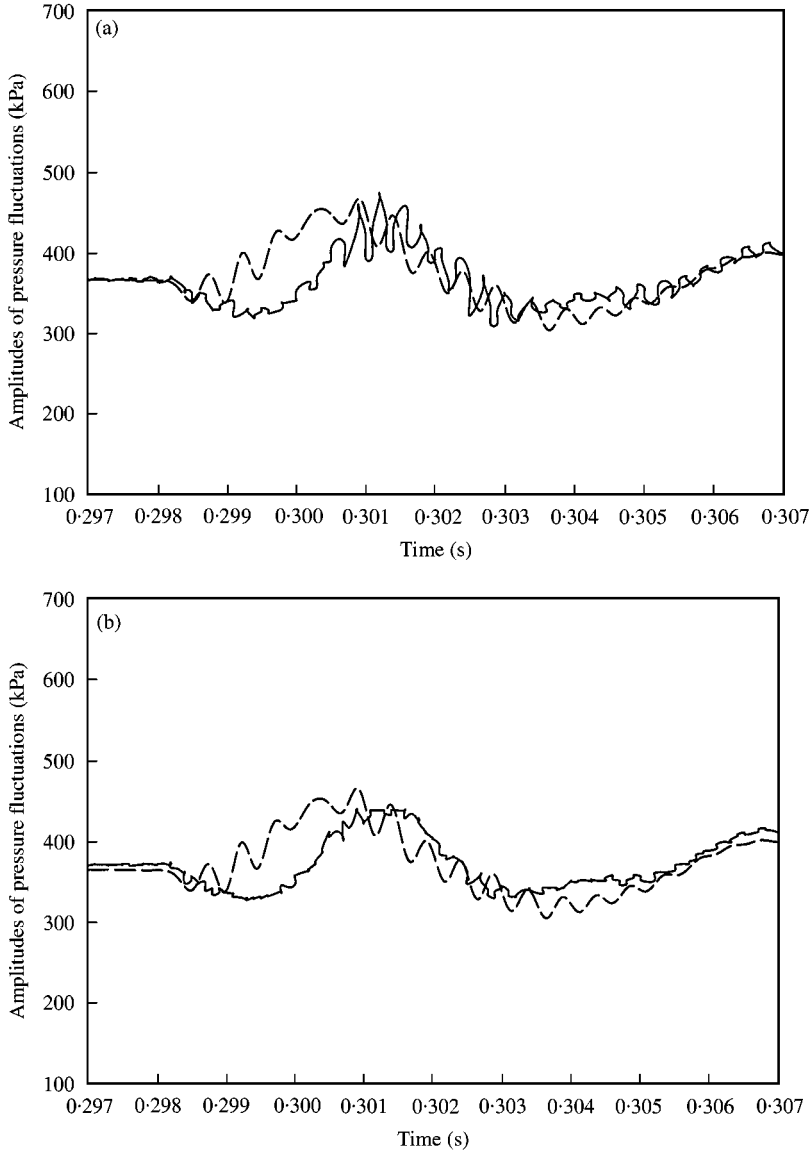

Figure 15. Comparison of pressure fluctuations inside the second injector with the fifth injector open only: (a) bottom; (b) top; ——, measured; – – –, calculated.

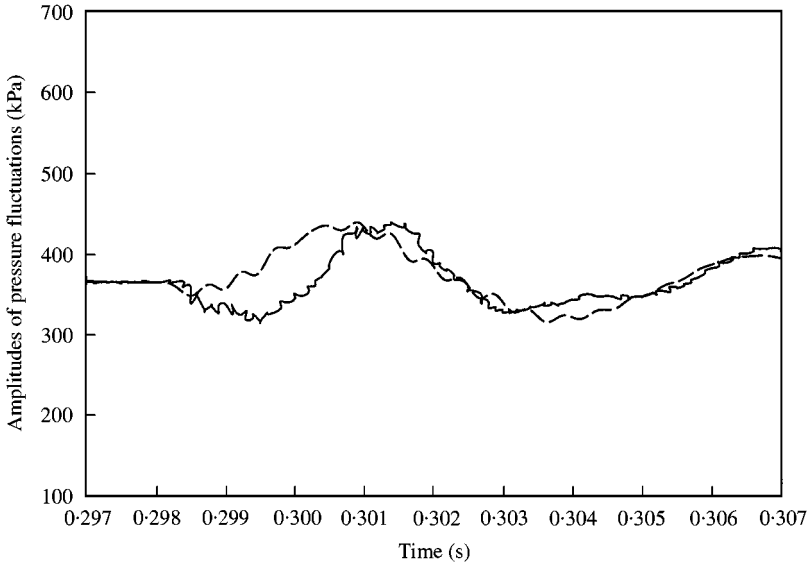

Figure 16. Comparison of pressure fluctuations inside the fuel line segment 2 with the fifth injector open only: ——, measured; – – –, calculated.

REFERENCES

1. Q. HU, S. F. WU, S. STOTTLER and R. RAGHUPATHI 1999 *Journal of Sound and Vibration* **245**, 801–814. Modeling of dynamic responses of an automotive fuel rail system. Part I: Injector.
2. R. H. SABERSKY, A. J. ACOSTA and E. G. HAUPTMANN 1971 *Fluid Flow*. New York: Macmillan Publishing Co., Inc.; Second edition.
3. R. H. F. PAO 1965 *Fluid Mechanics*. New York: John Wiley and Sons, Inc.
4. D. S. MILLER 1990 *Internal Flow Systems*. Cranfield, Bedford, UK: BHRA (Information Services); Second edition.
5. W. FLÜGGE 1962 *Handbook of Engineering Mechanics*. New York: McGraw-Hill Book Company, Chapter 39, pp. 24–31.
6. R. L. MOTT 1994 *Applied Fluid Mechanics*. New York: Maxwell Macmillan International.
7. M. B. ABBOTT and D. R. BASCO 1989 *Computational Fluid Dynamics: an Introduction for Engineers*. Harlow, Essex, England: Longman Scientific & Technical; New York, Wiley.
8. G. J. SHARPE 1994 *Solving Problems in Fluid Dynamics*. Harlow, Essex, England: Longman Scientific & Technical; New York: Wiley.
9. M. J. CROCKER 1998 *Handbook of Acoustics*. New York: John Wiley & Sons, Inc.